

# An EGSnrc investigation of the $P_{TP}$ correction factor for ion chambers in kilovoltage x rays

Daniel J. La Russa and D. W. O. Rogers

Carleton Laboratory for Radiotherapy Physics, Ottawa-Carleton Institute for Physics, Carleton University, Ottawa, ON, K1S 5B6, Canada

(Received 16 June 2006; revised 18 October 2006; accepted for publication 18 October 2006; published 17 November 2006)

As part of the standard practice for obtaining consistent ion chamber measurements with cavities open to the surrounding atmosphere, the raw measured response is corrected to the response at a reference temperature and pressure using the standard temperature-pressure correction factor ( $P_{TP}$ ). In this study, the EGSnrc Monte Carlo code was used to investigate the validity of the  $P_{TP}$  correction factor for kilovoltage x rays incident on various geometrically distinct ion chambers. The calculated  $P_{TP}$ -corrected chamber response deviated by over 2% relative to expected values for a 40 kV spectrum incident on a graphite thimble chamber at an air density typical of Mexico City. The relative deviation from the expected response was much worse for a large spherical graphite chamber, exceeding 16% at an air density of  $0.6 \text{ kg/m}^3$  ( $\approx 0.5 \text{ atm}$  at  $22^\circ \text{C}$ ) for the same beam energy. The breakdown of the  $P_{TP}$  correction factor was also observed for a 26 kV mammography spectrum incident on two mammography chambers. For  $^{60}\text{Co}$  beams, the  $P_{TP}$  correction factor behaved as expected. For day-to-day variations in pressure, only a negligible of the  $P_{TP}$  correction factor was observed with low x-ray energies. Factors contributing to the breakdown of the  $P_{TP}$  correction factor at low x-ray energies and large pressure variations, such as the range of electrons, the material of the wall, the chamber dimensions and air-photon interactions, are discussed in depth. © 2006 American Association of Physicists in Medicine. [DOI: 10.1118/1.2392407]

Key words: temperature-pressure correction, air pressure, Monte Carlo, dosimetry

## I. INTRODUCTION

When using ion chambers with cavities open to the atmosphere it is common practice<sup>1-3</sup> to correct the chamber response to the response under reference atmospheric conditions,  $M'$ , given by

$$M' = MP_{TP}, \quad (1)$$

where  $M$  is the charge collected by the ion chamber in the local environment, and  $P_{TP}$  is a correction factor used to relate ion chamber response measured at the temperature,  $T$ , and pressure,  $P$ , of the surrounding air to a set of reference conditions. Using the ideal gas law,  $P_{TP}$  can be shown to be

$$P_{TP} = \left( \frac{273.15 + T/^\circ \text{C}}{273.15 + T_0/^\circ \text{C}} \right) \left( \frac{P_0}{P} \right), \quad (2)$$

where  $T_0$  and  $P_0$  are the reference temperature and pressure, respectively. In North America, the reference temperature is  $22^\circ \text{C}$  (295.15 K) and the reference pressure is 101.325 kPa ( $\equiv 1 \text{ atm}$ , 760 mmHg), corresponding to a reference density of dry air,  $\rho_0 = 1.205 \text{ kg/m}^3$ .<sup>4</sup>  $P_{TP}$  is constructed such that  $\rho_0 = \rho P_{TP}$ ,<sup>5</sup> where  $\rho$  is the local air density.

The charge,  $M$ , collected by an ion chamber is the result of ionization produced by electrons as they travel through the cavity. Assuming that the energy deposited per unit charge released,  $(W/e)_{\text{air}}$ , is independent of beam quality, this ionization is directly proportional to the energy deposited by the electrons. For high-energy photon beams the majority of electrons producing ionization are assumed to emerge from

the wall of the chamber and have enough energy to cross the cavity. For low-energy beams the number of photon interactions in the air of the cavity contributing to the response is non-negligible. In either case, the energy deposited by an electron,  $E_{\text{dep}}$ , is

$$E_{\text{dep}} = \rho t \left( \frac{dE}{\rho dt} \right), \quad (3)$$

where  $t$  is the track length of an electron in the cavity, and  $(dE/\rho dt)_E$  is the mass-stopping power of the air appropriately averaged over the electron energy as it changes traversing  $t$ . The mass-stopping power is independent of the density of the air since the effect of density on collisional energy loss is completely negligible at the energies of interest ( $\leq 250 \text{ keV}$ ).<sup>6</sup> For electrons that completely cross the cavity, the average physical track length is, to a very good approximation, fixed, and the energy deposited is proportional to the density,  $\rho$ . From the relation  $\rho_0 = \rho P_{TP}$ , it follows that  $E_{\text{dep}}$ ,  $P_{TP}$ , and hence  $M'$ , are independent of  $\rho$  for a given beam energy.

Although the form of the  $P_{TP}$  correction factor may be theoretically justified using the above arguments, it has been observed to break down when applied to well ionization chambers used to determine the air kerma strength of brachytherapy seeds. Bohm *et al.*<sup>7</sup> and Griffin *et al.*<sup>8</sup> reported that the relative response to 20 keV photons was overcorrected by as much as 18% at low air pressures associated with regions of high altitude, and noted the discrepancies were related to the ranges of electrons and the material of the cham-

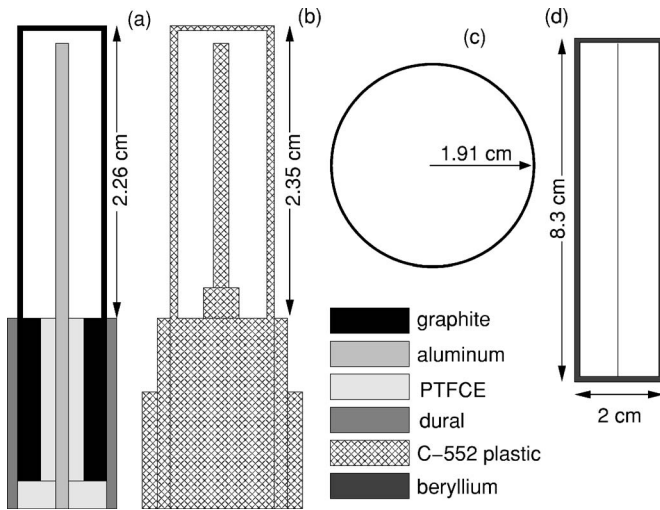


FIG. 1. EGSnrc models of (a) an NE 2571 chamber with  $0.061 \text{ g/cm}^2$  thick graphite walls and a cavity and Al electrode with  $0.68$  and  $0.1 \text{ cm}$  diameters, respectively. A  $0.59 \text{ g/cm}^2$  thick delrin buildup cap was included for calculations in a  $^{60}\text{Co}$  beam; (b) an Exradin A12 chamber with  $0.088 \text{ g/cm}^2$  thick C-552 plastic walls and inner diameter of  $0.71 \text{ cm}$ ; (c) A spherical chamber with  $0.085 \text{ g/cm}^2$  thick graphite walls and the same dimensions as the Exradin A4 chamber. The wall thickness was increased to  $0.5 \text{ g/cm}^2$  for  $^{60}\text{Co}$  calculations, and this chamber was also modeled using C-552 plastic as the wall material; (d) a monitor chamber used in the x-ray standard at NRCC, where the center line represents a  $0.27 \text{ mg/cm}^2$  thick aluminum electrode. The beryllium walls of this chamber are  $0.092 \text{ g/cm}^2$  thick.

ber wall. In principle, the same problems may exist for cavity ion chamber measurements used in kilovoltage x-ray beams. If this is the case, use of the standard  $P_{TP}$  correction with calibration coefficients in regions high above sea level (asl), such as Calgary ( $1000 \text{ m asl}$ ), Denver ( $1620 \text{ m asl}$ ), or Mexico City ( $2240 \text{ m asl}$ ) may be inappropriate.

In this article we investigate the application of the  $P_{TP}$  correction factor to ion chamber measurements of kilovoltage x-ray beams. The responses of four ion chambers, representing a range of dimensions and wall materials, were calculated as a function of air density using the Monte Carlo technique. Our results show that, for low-energy x rays, the  $P_{TP}$  correction factor does not properly account for changes in ion chamber response due to deviations of air density from reference conditions.

## II. CALCULATIONS

### A. Ion chambers

Several types of geometrically distinct ion chambers were investigated to elucidate any dependence of the  $P_{TP}$  correction factor on the cavity dimensions and wall materials. Cross sections of these chambers as modeled in our Monte Carlo calculations are shown in Figs. 1 and 2. The Farmer-type thimble chambers in Fig. 1 are based on the NE 2571 chamber [Fig. 1(a)] and the Exradin A12 [Fig. 1(b)]. The former model is taken from previous investigations.<sup>9,10</sup> Figure 1(c) shows an idealized spherical ion chamber with graphite walls. The radial dimensions of this chamber are the same as the Exradin A4 chamber made with C-552 air-

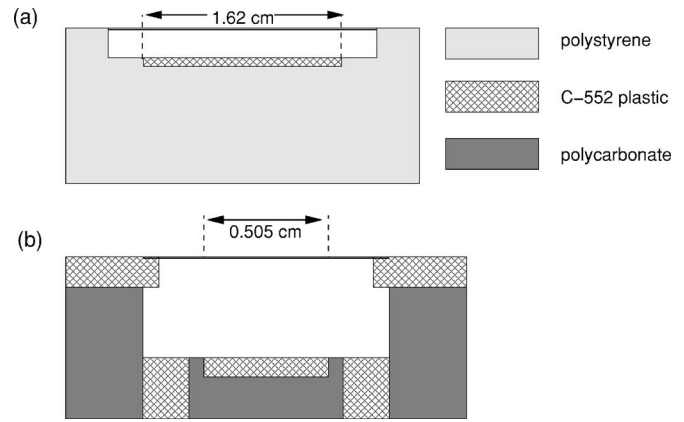


FIG. 2. Geometries of the Capintec PS-033 chamber (a) and the Exradin Magna A600 chamber (b). Mylar was used as the front wall material of the PS-033 chamber and is  $0.5 \text{ mg/cm}^2$  thick in this model. The front wall of the Magna A600 chamber is a  $0.0036 \text{ g/cm}^2$  thick kapton window. The collecting regions of these chambers are defined by the dashed lines.

equivalent plastic. Calculations with this geometry were also done using C-552 plastic as the wall material. The chamber in Fig. 1(d) is based on the parallel-plate monitor chamber used with the x-ray standard at the Ionizing Radiation Standards laboratory at the National Research Council of Canada (IRS-NRCC).

Figure 2 shows our models of two commonly used mammography chambers, the Capintec PS-033 [Fig. 2(a)], and the Magna A600 from Standard Imaging [Fig 2(b)]. The collecting regions of these chambers are defined by the front and back wall and the dashed lines. For each of the chambers, Table I lists the mean chord length,  $L$ , calculated from the relation  $L=4V/S$ , where  $V$  is the volume of the cavity and  $S$  is the surface area.<sup>5</sup> Also listed are the energies of electrons having a range equal to  $L$  at an air density of  $\rho_0$ .

### B. X-ray spectra

Representative narrow (NS) and high-rate (HR) x-ray spectra were obtained from a catalog by Ankerhold.<sup>11</sup> The average photon energies of these spectra are listed in Table

TABLE I. Mean chord lengths ( $L$ ) for the chambers shown in Fig. 1 and Fig. 2, calculated using the prescription  $L=4V/S$ , where  $V$  is the volume of the cavity and  $S$  is the surface area (Ref. 5). For the mammography chambers,  $L$  was calculated for the collecting region only, defined by the dashed lines in Fig. 2(a) and 2(b). The corresponding energies of electrons with a continuous slowing down approximation (CSDA) range in air ( $R_{\text{CSDA}}$ ) equal to  $L$ , were obtained by interpolating data in Attix (Ref. 5).

Chamber model	$L$ (cm)	$e^-$ energy for $R_{\text{CSDA}}=L$ at $\rho_0$ (keV)
NE 2571	0.48	14.5
Exradin A12	0.52	15.2
spherical	2.55	38.4
NRCC monitor chamber	2.55	38.4
PS-033	0.37	12.5
Magna A600	0.10	5.8

TABLE II. Average photon energies for the narrow (NS) and high-rate (HR) x-ray spectra from the PTB (Ref. 11) used in this study. Also listed are the average electron energies emerging from a slab of graphite ( $0.073 \text{ g/cm}^2$ ), a slab of beryllium ( $0.092 \text{ g/cm}^2$ ), a slab of C-552 plastic ( $0.076 \text{ g/cm}^2$ ), along with the corresponding CSDA ranges in air for these mean energies. The average electron energies were calculated using FLURZnrc (Ref. 19) and the CSDA ranges were interpolated from range data in Attix (Ref. 5).

PTB spectra	Avg. photon energy (keV)	avg. $e^-$ energy			$R_{\text{CSDA}}$ (air) at $\rho_0$	
		Graphite	C-552 (keV)	Be	Graphite (cm)	Be
20 kV (HR)	13.1	8.6	8.7	8.5	0.20	0.19
40 kV (NS)	33.3	22.2	22.6	19.3	0.99	0.78
60 kV (NS)	47.9	27.1	30.4	17.0	1.40	0.63
120 kV (NS)	100.4	23.2	31.2	17.7	1.07	0.67
250 kV (NS)	207.1	54.1	57.0	52.3	4.56	4.33

II. For the mammography chambers, a 26 kV mammography spectrum was obtained from IPEM Report 78,<sup>12</sup> and is similar to the spectrum published by Boone *et al.*<sup>13</sup> A  $^{60}\text{Co}$  spectrum published by Mora *et al.*<sup>14</sup> was used for calculations with the NE 2571 and spherical chambers. With the exception of the NRCC monitor chamber, which made use of a parallel beam with a 2 cm beam radius, all calculations used a point source with a 100 cm source-to-surface distance (SSD) and a beam radius large enough to cover the entire chamber.

## C. Monte Carlo calculations

### 1. Structure of the calculations

With the exception of the continuous slowing down approximation (CSDA) ranges of electrons in air, all quantities in this study were computed using the EGSnrc Monte Carlo computer code.<sup>15–17</sup> The accuracy of EGSnrc for calculating the response of ion chambers in low-energy x-ray beams has been demonstrated previously.<sup>18</sup> Ion chamber response was calculated using the CAVRZnrc user code for the cylindrically symmetric chambers and the CAVSPHnrc user code for the spherical chambers.<sup>19</sup> The omission of a central electrode and stem from the spherical chambers in our model was due to the inability of CAVSPHnrc to model cylindrical shapes. Nevertheless, it is expected that the calculated response of these simplified models will adequately reflect the real response of spherical chambers of this size as long as the material of the neglected components is the same as the wall, and the volume of the cavity is comparatively larger.

The Monte Carlo calculated  $P_{TP}$ -corrected response of the various ion chambers was extracted from calculations of the dose to the air in the cavity,  $D_{\text{cav}}$ . Corrections for changes in air density are inherent in these calculations since  $D_{\text{cav}}$  is the ratio of  $E_{\text{dep}}$  over the mass of air in a fixed volume. Thus, to the extent that  $(W/e)_{\text{air}}$  is constant with respect to  $\rho$  for a given beam quality,

$$D_{\text{cav}} \propto M(\rho) \times P_{TP}, \quad (4)$$

where  $M(\rho)$  is the chamber response at an air density of  $\rho$ . The validity of the  $P_{TP}$  correction factor can thus be checked by varying the density of air in the calculation. To relate the

calculated results to physical models, additional Monte Carlo calculations of the spectra of electrons emerging from walls of various materials were done using the EGSnrc user code FLURZnrc.<sup>19</sup>

### 2. Cross-section data sets

To simulate a change in air pressure within the cavity, a series of interaction cross sections was created for dry-air densities ranging from  $0.602$  to  $1.566 \text{ kg/m}^3$ , corresponding to pressures ranging from  $0.5$  to  $1.3 \text{ atm}$  at  $22^\circ\text{C}$ . Setting up the calculations in this way is convenient and assumes that air density is directly related to pressure at a constant temperature. This assumption is valid to within  $0.1\%$  over the range of pressures used in this study according to van der Waals approximations for deviations from ideal conditions.<sup>20</sup> All data sets were based on the XCOM photon cross sections<sup>21–23</sup> and density-effect corrections prescribed by Berger and Seltzer<sup>24,25</sup> and ICRU Report 37.<sup>6</sup>

### 3. EGSnrc parameters

For calculations of ion chamber response, electrons and photons were followed down to a kinetic energy of  $1 \text{ keV}$ . That is, the lowest energy of secondary electrons created (AE) and the lowest energy of electrons tracked (ECUT) were both set to  $0.512 \text{ MeV}$  (rest mass plus  $1 \text{ keV}$ ). Likewise, the analogous values for photons (AP and PCUT) were set to  $0.001 \text{ MeV}$ . In order to calculate the contribution of photon interactions in the cavity to the response, ECUT was increased to  $0.800 \text{ MeV}$  in the walls of the chambers so only electrons set in motion in the cavity contributed to the response. In all calculations, Rayleigh scattering, atomic relaxations, electron impact ionization, photoelectric angular sampling, and bound Compton scattering were used at all times. The only time-saving options implemented were electron range rejection and a variance reduction technique known as photon splitting, with a splitting number of around  $30$ .<sup>19,26</sup>

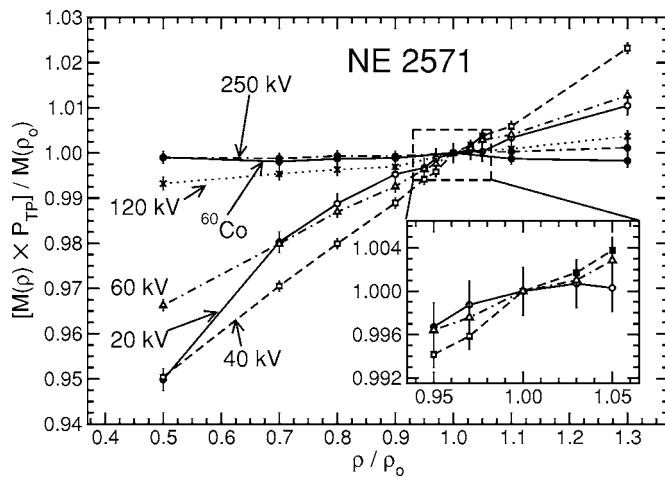


FIG. 3. EGSnrc-calculated responses of the NE 2571 chamber [Fig. 1(a)] as a function of air density for five PTB x-ray beam qualities and  $^{60}\text{Co}$ . The data points are inherently corrected for temperature and pressure ( $P_{TP}$ ) and normalized to unit response at a dry air density of  $1.205 \text{ kg/m}^3$ . The inset shows the data for the 20 kV (solid line), 40 kV (dashed line) and 60 kV (dotted line) for air densities ranging from  $\rho/\rho_0=0.95$  ( $1.145 \text{ kg/m}^3$ ) to  $\rho/\rho_0=1.05$  ( $1.265 \text{ kg/m}^3$ ), corresponding to a 5% deviation from reference temperature and pressure conditions.

### III. RESULTS

#### A. NE 2571 chamber

The EGSnrc-calculated response of the NE 2571 chamber as a function of air density is shown in Fig. 3. The data inherently include the  $P_{TP}$  correction and are normalized to unity at the reference air density of  $1.205 \text{ kg/m}^3$ . If the variation in the calculated response as a function of pressure was properly accounted for by the  $P_{TP}$  correction factor, the  $P_{TP}$ -corrected response would be unity as a function of air density. However, at an air density of  $\rho/\rho_0=0.76$ , typical of Mexico City, the calculated  $P_{TP}$ -corrected response is below unity by as much as 1.5% for the 20 and 60 kV spectra, and by over 2% for the 40 kV spectrum. The relative deviation for the 120 kV spectrum is much less, and the response is constant within 0.25% for the 250 kV and  $^{60}\text{Co}$  beams. The inset shows the calculated  $P_{TP}$ -corrected response for the 20, 40, and 60 kV, spectra over air densities ranging 5% above and below the reference density,  $\rho_0$ . Here, the relative deviation of the normalized response is as much as 0.5% for the 40 kV spectrum at  $\rho/\rho_0=0.95$ . Although this is quite substantial from the perspective of a primary or secondary standards laboratory, the pressure rarely deviates to that extent. In fact, pressure variations measured at the NRC over a 6 month period between May and November 2005 were within about 1.2% of the mean (100.32 kPa) at the 95% confidence level. Interpolating the data to within these limits brings the expected variation to more acceptable levels (0.1%), and so it is not surprising that problems associated with the  $P_{TP}$ -correction were not detected previously. For the 120, 250 kV and  $^{60}\text{Co}$  spectra, the calculated  $P_{TP}$ -corrected response is within 1% of unity over the range of air densities considered here.

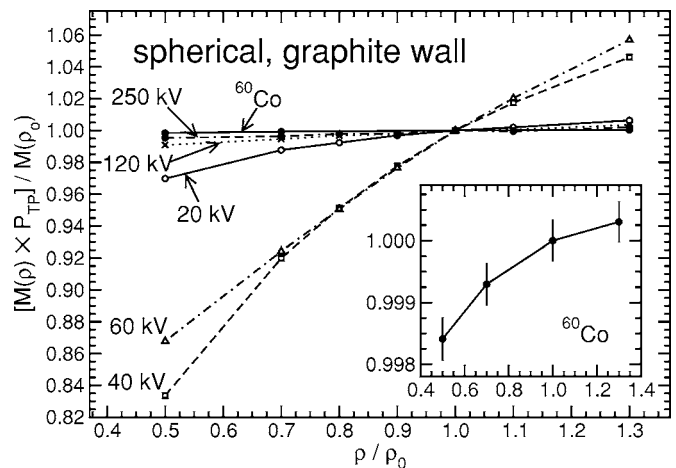


FIG. 4. As in Fig. 3 for the spherical chamber with graphite walls [Fig. 1(c)]. The inset in this figure shows the variation in the calculated  $P_{TP}$ -corrected response for  $^{60}\text{Co}$  over the whole range of air densities investigated here. Note that the range of the y axis is nearly 3 times greater than in Fig. 3. All relative uncertainties are 0.05% or smaller.

### B. Spherical chambers

#### 1. Graphite walls

Figure 4 shows the calculated  $P_{TP}$ -corrected response of the spherical chamber with graphite walls [Fig. 1(c)] as a function of air density, normalized to the response at  $\rho_0$ . Unlike the response for the NE 2571 chamber, the largest variation is seen for the 40 and 60 kV spectra, deviating from unity by roughly 17% and 13%, respectively, at an air density of  $\rho/\rho_0=0.5$ . The inset to Fig. 4 shows the relative calculated response function for the  $^{60}\text{Co}$  beam over the whole range of air densities. In this case the chamber can be regarded as a Bragg-Gray cavity since photon interactions in the is are negligible and the range of electrons is large compared to the dimensions of the chamber. Here, the slight variation with respect to air density is attributed to the variation in  $\Delta$ , the low-energy cutoff used in determining the Spencer-Attix stopping power ratio.<sup>27–29</sup>

#### 2. C-552 walls

Figure 5 shows results for the spherical chamber with C-552 air-equivalent plastic walls rather than graphite. In contrast to the spherical chamber with graphite walls, all normalized responses are within 0.7% of the response at the reference density. The largest deviation is seen for the 20 kV spectrum.

### C. Exradin A12

As in the case of the spherical chambers, the EGSnrc-calculated response of the Exradin A12 Farmer-type thimble chamber with C-552 plastic walls [Fig. 1(b)] is also substantially different from the graphite-walled equivalent; the NE 2571 chamber. The largest deviation from unity in the normalized  $P_{TP}$ -corrected response is observed for the 20 kV spectrum, but it is less than 1% low at  $\rho/\rho_0=0.5$  (Fig. 6).

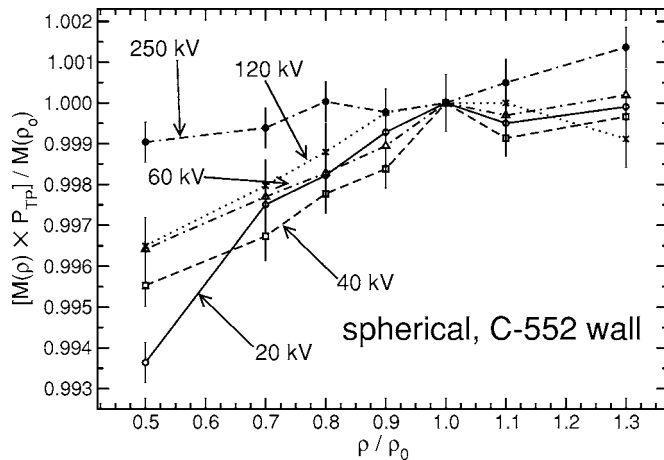


FIG. 5. As in Fig. 3 but for the spherical chamber with C-552 plastic walls. Note the much reduced range of the y axis.

The normalized response due to the remaining x-ray spectra is nearly constant over the whole range of air densities tested.

## D. NRC monitor chamber

### 1. NRC monitor chamber with aluminum electrode

Figure 7 shows the calculated  $P_{TP}$ -corrected response for the five spectra as a function of air density for the NRC monitor chamber [Fig. 1(d)] normalized at  $\rho/\rho_0=1.0$ . Here we observe a deviation above unit response at low air densities for the 20 and 40 kV spectra by as much as 10% and 2%, respectively. Also, the substantial variation for the 250 kV spectrum is unique to this chamber.

### 2. NRC monitor chamber without aluminum electrode

To investigate the influence of the aluminum electrode on the response of the monitor chamber, the calculations were repeated with this electrode removed from the geometry. The

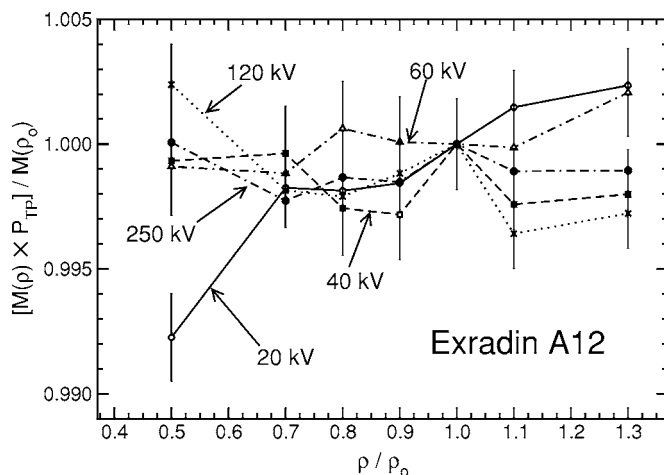


FIG. 6. As in Fig. 3 for the Exradin A12 chamber, which is a Farmer-type thimble chamber with C-552 air-equivalent walls [Fig. 1(b)].

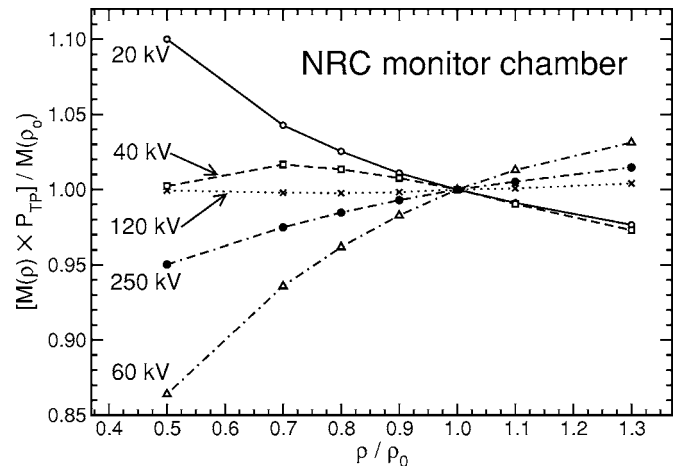


FIG. 7. As in Fig. 3 for the NRC monitor chamber used in the primary x-ray standard at NRC in Ottawa [Fig. 1(d)]. All statistical relative uncertainties are 0.05% or smaller.

normalized  $P_{TP}$ -corrected response for this modified chamber is shown in Fig. 8. None of the normalized response functions for the five PTB spectra tested deviated above unity for low relative air densities. Furthermore, the largest variation in relative response is observed for this chamber geometry, with the 60 kV spectrum deviating below unity by nearly 24% at an air density of  $\rho/\rho_0=0.5$ . The response for the 120 kV spectrum is relatively constant over the whole range of air densities tested, as in the case where the electrode is present. For these same air densities, the responses of the 250 and 40 kV spectra varied by 9% and 25%, respectively.

## E. Mammography chambers

For the Capintec PS-033 and Exradin Magna A600 chambers, only the 26 kV mammography spectrum was used. The average photon energy of this spectrum is 13.5 keV. Calculated  $P_{TP}$ -corrected responses of both these chambers are shown in Fig. 9, which demonstrates that the breakdown of

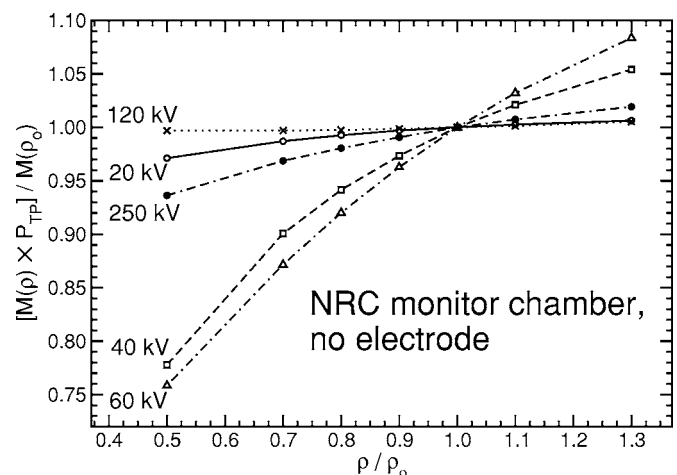


FIG. 8. As in Fig. 7 for the NRC monitor chamber [Fig. 1(d)] with no aluminum electrode.

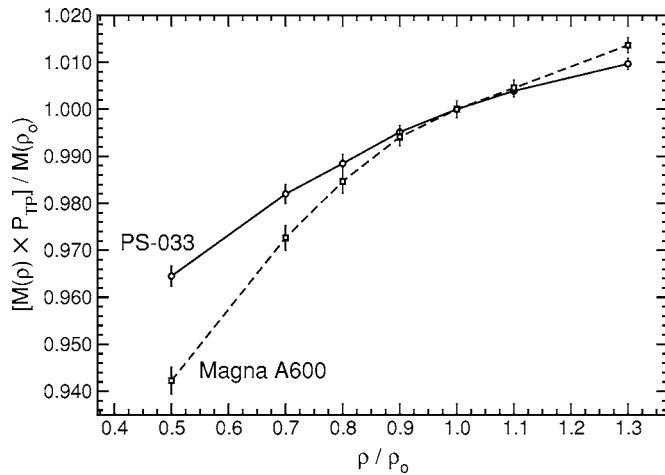


Fig. 9. Normalized  $P_{TP}$ -corrected response for the Capintec PS-033 [Fig. 2(a)] and Exradin Magna A600 [Fig. 2(b)] as a function of air density, calculated using EGSnrc. A 26 kV mammography spectrum from IPEM Report 78 (Ref. 12) was investigated with these chambers.

the  $P_{TP}$  correction factor also applies to mammography chambers. The extent of the breakdown is chamber dependent, with relative deviations below the expected response exceeding 3% for the PS-033 chamber, and approaching 5% for the Magna A600 at  $\rho/\rho_0=0.5$ .

#### IV. DISCUSSION

The Monte Carlo calculations presented in the previous section demonstrate that the standard temperature-pressure correction factor breaks down for x-ray beam qualities as high as 250 kV in some cases. These results also indicate that the extent of the breakdown has a strong dependence on beam quality. The following sections discuss how the extent of the breakdown depends on several other contributing factors, including the range of electrons, material of the wall and electrode, and the fraction of photons interactions in the cavity.

#### A. Influence of electron ranges on chamber response

Since ion chamber response is the result of ionization produced by electrons as they cross the cavity, one might expect the failure of the  $P_{TP}$  correction factor to be directly related to the range of electrons set in motion in the wall by the incident beam. For instance, consider the hypothetical situation where the electrons have a range just sufficient to cross the cavity at an air density of  $\rho/\rho_0=0.5$ . As the air density is increased, the electrons that escaped the cavity at the lower density are now stopped, depositing all of their energy as opposed to depositing an amount of energy which is proportional to the air density. So, the measured charge becomes constant as the density increases further, which means  $MP_{TP}$  decreases instead of being constant as expected. Alternatively, if the number of electrons that stop in the cavity continues to increase as the pressure increases, more energy is deposited beyond what is expected if they had crossed since the stopping power also increases as the electron slows to a stop. As a result, the  $P_{TP}$ -corrected response increases with increasing air density. In either case, Eq. (3) no longer holds and the response is not proportional to  $\rho t$ .

To explore the above notion in detail the EGSnrc user-code FLURZnrc was used to calculate the spectra of electrons emerging from slabs of graphite, C-552 plastic, and beryllium. The results for the four lowest-energy photon beams (20–120 kV) are shown in Fig. 10. The thicknesses of the slabs are equivalent to those used in the walls of the NE 2571 (graphite), spherical (C-552 plastic), and NRC monitor (beryllium) chambers. Table II lists the average electron energies along with the corresponding ranges in dry air at the reference density ( $\rho_0$ ) for each of the five PTB spectra. The average energies of electrons emerging from each of the three wall materials does not increase in proportion to the incident x-ray beam energy. This makes it difficult to account for the extent of the breakdown in the  $P_{TP}$  correction factor in terms of electron ranges alone. As an example, contrary to what is observed (Fig. 3), it would be expected that the rela-

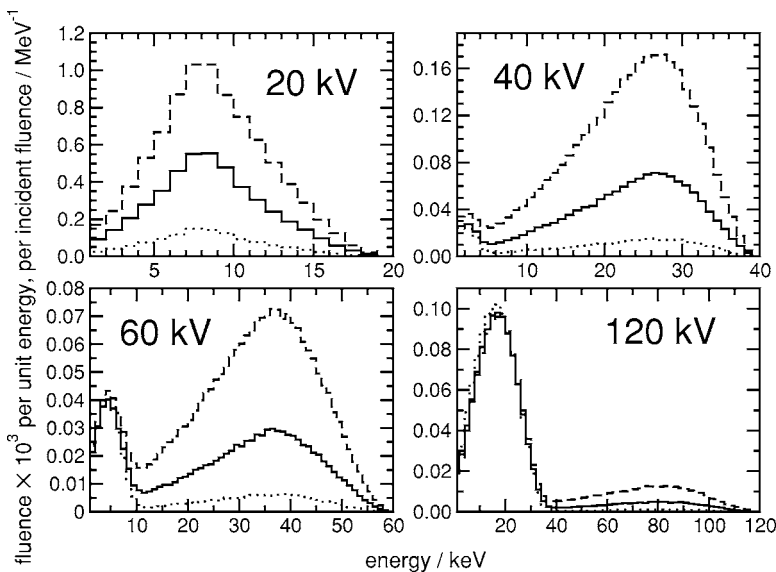


Fig. 10. EGSnrc-calculated spectra of electrons emerging from slabs of beryllium (dotted line,  $0.09 \text{ g/cm}^2$ ), graphite (solid line,  $0.06 \text{ g/cm}^2$ ), and C-552 air-equivalent plastic (dashed line,  $0.09 \text{ g/cm}^2$ ) upon irradiation by the broad-beam PTB spectra listed in Table II. The low-energy peaks (absent in 20 kV case) are Compton secondaries, which are roughly the same intensity in each material, and become relatively more important as the photon energy increases due to the increase in Compton cross section. The higher-energy electrons are from the photoelectric interactions, which are strongly material dependent and relatively less important at higher photon energies. The distribution of the high-energy peaks produced by the 40, 60, and 120 kV beams are similar for each material but differ significantly in intensity.

tive response of the 20 kV beam incident on the NE 2571 chamber would be different from that due to the 40 kV spectrum since the respective average electron energies differ by about 50%, and the corresponding distributions of electron energies differ even more significantly. Similarly, for the spherical graphite chamber, it would be expected that the relative responses of the 40 and 60 kV beams (Fig. 4) be more dissimilar owing to the differences in the corresponding spectra of electrons emerging from the wall. On the other hand, by considering only the average electron energies, the 40 and 60 kV beams should exhibit deviations in their relative response comparable to the 120 kV spectrum for this chamber. This is clearly not the case. Similar difficulty also arises when attempting to explain the results for the mammography chambers (e.g., the energy needed by an electron to travel a distance  $L$  through the cavity is less for the Magna A600 than it is for the PS-033) and the NRC monitor chamber with and without the aluminum electrode in terms of electron ranges. Thus, although the breakdown of the  $P_{TP}$  correction factor is associated with the range of electrons, the magnitude of the breakdown is influenced by other factors.

## B. Influence of wall material

The influence of wall material can be seen by comparing the response of the chambers with graphite and air-equivalent C-552 plastic walls along with the spectra of electrons emerging from the respective materials. With the exception of the 120 kV beam, the average energies and corresponding ranges of electrons emerging from C-552 plastic are similar to those of graphite for the respective beam qualities (Table II). However, despite these similarities, almost no breakdown of the  $P_{TP}$  correction factor is observed for the chambers with C-552 plastic walls (Figs. 5 and 6), even when the range of electrons is short in comparison to the mean chord length of the cavity. This may be explained using the theory of Fano, which states that for an infinite, homogeneous medium in a uniform field of indirectly ionizing radiation with negligible attenuation, the field of secondary radiation is also uniform and independent of density variations in the medium.<sup>5,30</sup> Thus, ignoring the effects of attenuation, chambers with air-equivalent walls will always have charged-particle equilibrium between the chamber wall and the air in the cavity regardless of air density, and we should not expect any variation in the  $P_{TP}$ -corrected response as a function of  $\rho$ . The results shown in Figs. 5 and 6 for the spherical and thimble chambers with C-552 plastic walls are consistent with this analysis within 1% for all beam qualities. A similar result was also observed by Bohm *et al.*<sup>7</sup> when comparing the Monte Carlo calculated response of realistic well-ionization chambers with hypothetical chambers of the same dimensions made with C-552 plastic walls.

Unlike the chambers made of C-552 plastic, no charged particle equilibrium exists between the wall and the air in the cavity for chambers with non-air-equivalent walls. The degree of disequilibrium is related to the extent that the photon cross sections between the material of the wall and air are different. Figure 11 shows the ratio of photon cross sections

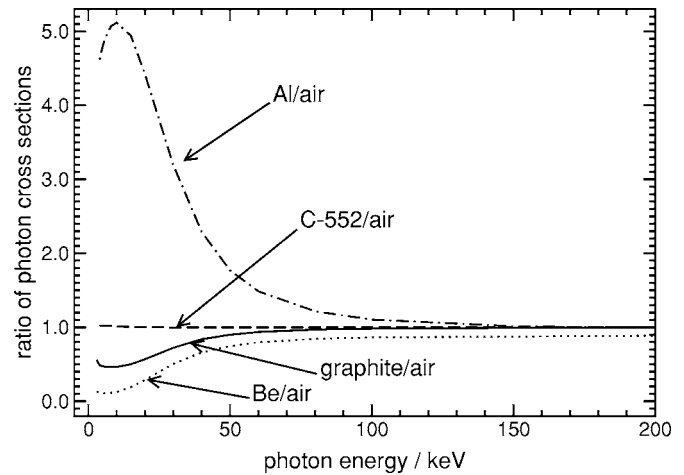


FIG. 11. Ratios of the total photon interaction cross sections (Refs. 21 and 22) as a function of photon energy for aluminum, beryllium, graphite, and C-552 air-equivalent plastic with respect to air. Similar data for mylar and kapton ratios to air are less than unity, with the ratio with mylar closer to unity.

of several materials with air. At the photon energies considered in this study, the mismatch in the photon cross sections between graphite and air is substantial,<sup>31</sup> differing by as much as a factor of 2 at 10 keV. The difference between the photon cross sections of beryllium and air is even greater, approaching a factor of 10 at 5 keV and only converging to within 10% at energies above 2 MeV. In general, the magnitude of breakdown of the  $P_{TP}$  correction factor for a given energy correlates with the extent that the photon cross sections between the wall and the air are different. Exceptions to this apply to the 20 kV beam incident on the chambers in Fig. 1, for which the overall variation is often less than the variation exhibited by higher energy beams despite there being a larger mismatch in air/wall cross sections at lower energies (Figs. 4 and 8). This can be explained by considering the fraction of the response that comes from photon interactions in the cavity, which is discussed in the next section. Other exceptions apply to the chambers with aluminum electrodes (NE 2571 and NRC monitor chamber) since, unlike the other materials considered here, aluminum has larger photon cross sections than air at low energies and tends to have a compensating effect or even an overcompensating effect for the 20 and 40 kV spectra incident on the NRC monitor chamber.

## C. Influence of $F_{\text{air}}$

It has been demonstrated that the breakdown of the  $P_{TP}$  correction factor is contingent on the combination of short electron ranges and a mismatch in photon cross sections between the wall and the air. However, the overall magnitude of the breakdown is also influenced by the fraction of the response due to photon interactions in the air of the cavity, denoted here as  $F_{\text{air}}$ . Ma and Nahum,<sup>32</sup> as well as Borg *et al.*,<sup>31</sup> have investigated  $F_{\text{air}}$  for Farmer-type thimble chambers, and have shown it to be nonlinear as a function of incident photon energy. We have approximated  $F_{\text{air}}$  as the

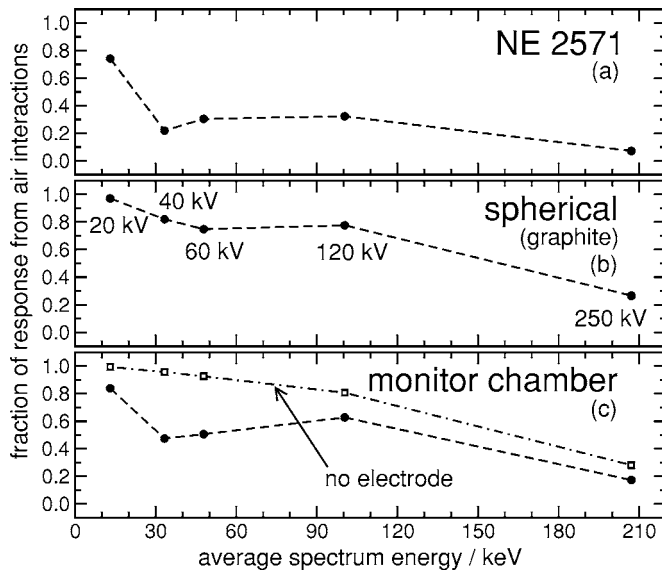


FIG. 12. Fraction of response due to photon interactions in the cavity ( $F_{\text{air}}$ ) as a function of the average photon energy for the NE 2571 chamber (a), spherical graphite chamber (b), and NRC monitor chamber (c) with (dashed line) and without (dashed and dotted line) the aluminum electrode. The average photon energies refer to those listed in Table II for the five PTB spectra used in this study. The corresponding beam qualities are shown in (b).  $F_{\text{air}}$  is estimated as the ratio of chamber response with high and low values of ECUT in the chamber walls and electrode, and is calculated at an air density of  $\rho/\rho_0=1$ . Computing  $F_{\text{air}}$  in this way ignores the contribution from backscattered electrons which is assumed to be negligible. Previous studies (Refs. 31 and 32) suggest a peak in  $F_{\text{air}}$  around a mean energy of 80 keV. However, a beam quality with an average energy of 80 keV was not considered here.

ratio of calculated responses with high and low values of ECUT in the walls and electrode of the chamber. Specifically,

$$F_{\text{air}} \approx \frac{M(\text{ECUT} = 800 \text{ keV in walls})}{M(\text{ECUT} = 512 \text{ keV everywhere})}. \quad (5)$$

The high ECUT values (800 keV) inhibit electron transport in the regions where it is applied, so the calculated response is entirely due to photon interactions in the cavity. Figure 12 shows values of  $F_{\text{air}}$  for the three chamber geometries as a function of the average photon energy for each of the PTB beam qualities (Table II). In each case  $F_{\text{air}}$  is highest for the 20 kV beam, approaching unity for the spherical graphite chamber and NRC monitor chamber with no electrode. These large values of  $F_{\text{air}}$  reduce the impact that non-air-equivalent walls have on the breakdown of the  $P_{TP}$  correction factor since a large portion of the response is from the “air-equivalent” air. This explains why the variation in the calculated  $P_{TP}$ -corrected response of the spherical graphite chamber and NRC monitor chamber with no electrode is less at 20 kV than at 40 and 60 kV, where  $F_{\text{air}}$  is considerably lower. This same reasoning also explains the relative variations in the  $P_{TP}$ -corrected response due to the 120 and 250 kV beams for the NRC monitor chamber with no electrode. Similar arguments can be made for the NE 2571 and NRC monitor chambers; however, fully accounting for the results in this way is complicated by the aluminum elec-

trodes. Regardless, in situations where the mean range of electrons is short compared with the dimensions of the cavity, it is clear that one must consider the contribution of both photon interactions in the cavity and the material of the chamber wall toward any breakdown in the  $P_{TP}$  correction factor.

#### D. Proposed experimental verification

Having established the causes of the breakdown of the  $P_{TP}$  correction factor using Monte Carlo simulations, it is worthwhile to consider a method of experimental verification. One approach is to measure the calibration coefficient for a chamber in labs situated at different altitudes using the same set of beam energies. Although straightforward, this approach ignores the possibility that primary standards and transfer standards may have similar problems associated with the  $P_{TP}$  correction factor. Additional issues related to inconsistencies between beam qualities from place to place may also complicate these comparisons, but would not be a major concern for chambers with  $N_K$  values that do not fluctuate significantly with changes in beam quality.

In order to circumvent the problems mentioned above, the ratio of responses for two geometrically distinct chambers (different wall materials and chamber dimensions) could be compared at different altitudes. This eliminates the need for primary or transfer standards. Alternatively, one could measure the response of chambers in an environmental chamber under precise control of the temperature and pressure. This allows comparisons to be made in one location but presents many challenges in controlling and determining the pressure and temperature within the system. Regardless, if the  $P_{TP}$ -corrected response of both chambers is linear with respect to air density, then so should the ratio of their respective  $P_{TP}$ -corrected responses. Therefore, any deviation in this normalized ratio from unity is an indication that the  $P_{TP}$  correction factor is breaking down for at least one of the chambers. In principle, if both normalized  $P_{TP}$ -corrected responses of the chambers are deviating the same way, then the possibility exists that problems with the  $P_{TP}$  correction factor will not be reflected in the ratio of response since the effect of each chamber will cancel out. Such problems can be avoided if one of the chambers is made of C-552 plastic walls, such as the Exradin A12, assuming the  $P_{TP}$ -corrected response is as stable as predicted here.

Figure 13 shows the ratio of responses as a function of  $\rho/\rho_0$  for the NE 2571 chamber and Exradin A12 chamber predicted using the results for Fig. 3 and Fig. 6 for the five PTB spectra considered in this investigation. The deviation of  $M^{NE\ 2571}/M^{A12}$  is about 4.5% below unity for the 20 and 40 kV spectra and 3% for the 60 kV spectrum at  $\rho/\rho_0=0.5$ . Thus, an NE 2571 chamber calibrated at NRC in Ottawa, at roughly the standard temperature and pressure conditions, is predicted to underestimate the air kerma in Mexico City, corresponding to an air density of  $\rho/\rho_0=0.78$ , by about 2% for a 40 kV spectrum. The situation is less severe in Calgary, Alberta ( $\rho/\rho_0=0.88$ ), where a roughly 1% underestimation would occur for the same beam quality. These predictions

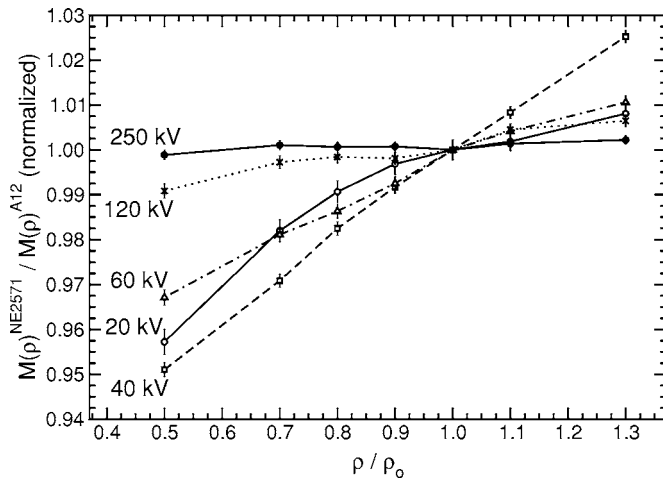


FIG. 13. Ratio of responses between the NE 2571 chamber (Fig. 3) and the Exradin A12 (Fig. 6) chambers as a function of air density for the five PTB spectra listed in Table II.

ignore contributions from impurities in or on the walls of the chambers. However, calculations involving impurities, incorporated according to prescriptions of a previous study,<sup>18</sup> did not appear to have a large effect on the response as a function of air density, even though changes in the absolute response were significant (data not shown).

Given the extent of the breakdown of the  $P_{TP}$  correction factor indicated in Fig. 13, it is interesting to note that this problem has not been previously reported by either primary or secondary standards laboratories. This may be due to the fact that comparisons between primary standards labs with a single type of ion chamber do not involve appreciable differences in air density. It is also possible that such discrepancies were not identified by standards labs at high altitudes (e.g., in Mexico City) if they consistently use the same calibrated ion chamber as their standard, or the chambers involved always had air-equivalent walls. Presumably, problems with the  $P_{TP}$  correction factor would be detected in the latter case by comparing the ratio of measurements with two distinctly different ion chambers in a standards lab at altitude with the ratio of measurements at sea level.

## V. CONCLUSIONS

The EGSnrc Monte Carlo code was used to compute the  $P_{TP}$ -corrected response of several geometrically distinct ion chambers irradiated by five low-energy PTB x-ray spectra and one IPEM mammography spectrum. Our calculations indicate that the standard  $P_{TP}$  correction factor may break down when the ranges of electrons are short relative to the dimensions of the cavity in chambers with non-air-equivalent walls. The extent of the breakdown is also influenced by the mismatch of photon cross sections between the chamber wall and air, and the fraction of photon interactions in the cavity contributing to the response. For chambers made with C-552 plastic walls, the  $P_{TP}$  correction was accurate within 1% over the range of air densities evaluated, at least to the extent that C-552 plastic is air-equivalent in terms of the photon cross

sections. Based on this result, it is advised that the use of chambers with air-equivalent walls be given priority at low x-ray energies when variations in air pressure are significant. This especially applies to regions of high altitude where air densities may differ significantly from those at the standards laboratory where the chamber was calibrated.

## ACKNOWLEDGMENTS

This research has been enabled by the use of WestGrid computing resources, which are funded by the Canada Foundation for Innovation, Alberta Innovation and Science, BC Advanced Education, and participating research institutions. The authors wish to acknowledge support from the Natural Sciences and Engineering Research Council of Canada (NSERC) and the Canada Research Chairs program. We would also like to thank Pat Saull for detailed data on the air pressure variations in the Ottawa region, Brian Hooten for providing us with details about the Exradin Magna A600 chamber, as well as Malcolm McEwen, Carl Ross, and members of the Carleton Laboratory for Radiotherapy Physics (CLRP) for their helpful comments regarding this article.

<sup>a</sup>Electronic mail: dlarussa@physics.carleton.ca

<sup>b</sup>Electronic mail: drogers@physics.carleton.ca

<sup>1</sup>P. R. Almond, P. J. Biggs, B. M. Coursey, W. F. Hanson, M. S. Huq, R. Nath, and D. W. O. Rogers, "AAPM's TG-51 protocol for clinical reference dosimetry of high-energy photon and electron beams," *Med. Phys.* **26**, 1847–1870 (1999).

<sup>2</sup>C.-M. Ma, C. W. Coffey, L. A. DeWerd, R. Nath, C. Liu, S. M. Seltzer, and J. Seuntjens, "AAPM protocol for 40–300 kV x-ray beam dosimetry in radiotherapy and radiobiology," *Med. Phys.* **28**, 868–893 (2001).

<sup>3</sup>IAEA, *Absorbed Dose Determination in Photon and Electron Beams: An International Code of Practice*, Volume 277 of Technical Report Series (IAEA, Vienna, 1987).

<sup>4</sup>D. R. Lide, *CRC Handbook of Chemistry and Physics*, 80th ed. (CRC, Boca Raton, FL, 2000).

<sup>5</sup>F. H. Attix, *Introduction to Radiological Physics and Radiation Dosimetry* (Wiley, New York, 1986).

<sup>6</sup>ICRU, "Stopping powers for electrons and positrons," ICRU Report 37, ICRU, Bethesda, MD, 1984.

<sup>7</sup>T. D. Bohm, S. L. Griffin, J. Paul, M. DeLuca, and L. A. DeWerd, "The effect of ambient pressure on well chamber response: Monte Carlo calculated results for the HDR 1000 Plus," *Med. Phys.* **32**, 1103–1114 (2005).

<sup>8</sup>S. L. Griffin, L. A. DeWerd, J. A. Micka, and T. D. Bohm, "The effect of ambient pressure on well chamber response: Experimental results with empirical correction factors," *Med. Phys.* **32**, 700–709 (2005).

<sup>9</sup>L. A. Buckley, I. Kawrakow, and D. W. O. Rogers, "An EGSnrc investigation of cavity theory for ion chambers measuring air kerma," *Med. Phys.* **30**, 1211–1218 (2003).

<sup>10</sup>L. A. Buckley, I. Kawrakow, and D. W. O. Rogers, "CSnrc: Correlated sampling Monte Carlo calculations using EGSnrc," *Med. Phys.* **31**, 3425–3435 (2004).

<sup>11</sup>U. Ankerhold, "Catalogue of X-ray spectra and their characteristic data -ISO and DIN radiation qualities, therapy and diagnostic radiation qualities, unfiltered X-ray spectra," Technical Report PTB-Dos-34, Physikalisch Technische Bundesanstalt, Braunschweig, Germany, 2000.

<sup>12</sup>K. Cranley, B. J. Gilmore, G. W. Fogarty, and L. Desponds, "IPEM Report 78: Catalogue of diagnostic x-ray spectra and other data," (CD-Rom edition 1997) (Electronic version prepared by D. Sutton), Technical Report Report 78, The Institute of Physics and Engineering in Medicine (IPEM), York, 1997.

<sup>13</sup>J. M. Boone, T. Yu, and A. Seibert, "Mammography spectrum measurement using x-ray diffraction device," *Phys. Med. Biol.* **43**, 2569–2582 (1998).

<sup>14</sup>G. Mora, A. Maio, and D. W. O. Rogers, "Monte Carlo simulation of a

- typical  $^{60}\text{Co}$  therapy source," *Med. Phys.* **26**, 2494–2502 (1999).
- <sup>15</sup>I. Kawrakow, "Accurate condensed history Monte Carlo simulation of electron transport. I. EGSnrc, the new EGS4 version," *Med. Phys.* **27**, 485–498 (2000).
- <sup>16</sup>I. Kawrakow and D. W. O. Rogers, "The EGSnrc Code System: Monte Carlo simulation of electron and photon transport," Technical Report PIRS-701, National Research Council of Canada, Ottawa, Canada (2000). (see <http://www.irs.inms.nrc.ca/inms/irs/EGSnrc/EGSnrc.html>).
- <sup>17</sup>I. Kawrakow, E. Mainegra-Hing, and D. W. O. Rogers, "EGSnrcMP: The multi-platform environment for EGSnrc," Technical Report PIRS-877, National Research Council of Canada, Ottawa, Canada, 2003.
- <sup>18</sup>J. P. Seuntjens, I. Kawrakow, J. Borg, F. Hobeila, and D. W. O. Rogers, "Calculated and measured air-kerma response of ionization chambers in low and medium energy photon beams," in *Recent Developments in Accurate Radiation Dosimetry, Proceedings of an International Workshop*, edited by J. P. Seuntjens and P. Mobit (Medical Physics Publishing, Madison WI, 2002), pp. 69–84.
- <sup>19</sup>D. W. O. Rogers, I. Kawrakow, J. P. Seuntjens, and B. R. B. Walters, "NRC User Codes for EGSnrc," Technical Report PIRS-702, National Research Council of Canada, Ottawa, Canada (2000). (see <http://www.irs.inms.nrc.ca/inms/irs/EGSnrc/EGSnrc.html>).
- <sup>20</sup>P. Atkins, *Physical Chemistry: Sixth Edition* (W. H. Freeman, New York, 1999).
- <sup>21</sup>M. J. Berger and J. H. Hubbell, "XCOM: Photon Cross Sections on a Personal Computer," Report NBSIR87-3597, NIST, Gaithersburg, MD, 1987.
- <sup>22</sup>M. J. Berger, J. H. Hubbell, S. M. Seltzer, J. S. Coursey, and D. S. Zucker, "XCOM: Photon cross section database (version 1.2)," Report, NIST, Gaithersburg, MD; see <http://physics.nist.gov/xcom>
- <sup>23</sup>F. Hobeila and J. P. Seuntjens, "Effect of XCOM photoelectric cross-sections on dosimetric quantities calculated with EGSnrc, IAEA-CN-96/17P," in Vol 1, *Proceedings of International Symposium on Standards and Codes of Practice in Medical Radiation Dosimetry* (IAEA, Vienna, 2003), pp. 177–186.
- <sup>24</sup>M. J. Berger and S. M. Seltzer, "Stopping power and ranges of electrons and positrons," NBS Report NBSIR 82-2550-A, 2nd ed. (1983).
- <sup>25</sup>S. Duane, A. F. Bielajew, and D. W. O. Rogers, "Use of ICRU-37/NBS collision stopping powers in the EGS4 system," NRCC Report PIRS-0173, Ottawa, March (1989).
- <sup>26</sup>I. Kawrakow and M. Fippel, "Investigation of variance reduction techniques for Monte Carlo photon dose calculation using XVMC," *Phys. Med. Biol.* **45**, 2163–2184 (2000).
- <sup>27</sup>D. V. Cormack and H. E. Johns, "The measurement of high-energy radiation intensity," *Radiat. Res.* **1**, 133–157 (1954).
- <sup>28</sup>G. N. Whyte, "Measurement of the Bragg-Gray stopping power correction," *Radiat. Res.* **6**, 371–379 (1957).
- <sup>29</sup>F. H. Attix, L. DeLa Vergne, and V. H. Ritz, "Cavity ionization as a function of wall material," *J. Res. Natl. Bur. Stand.* **60**, 235–243 (1958).
- <sup>30</sup>U. Fano, "Note on the Bragg-Gray cavity principle for measuring energy dissipation," *Radiat. Res.* **1**, 237–240 (1954).
- <sup>31</sup>J. Borg, I. Kawrakow, D. W. O. Rogers, and J. P. Seuntjens, "Monte Carlo study of correction factors for Spencer-Attix cavity theory at photon energies at or above 100 keV," *Med. Phys.* **27**, 1804–1813 (2000).
- <sup>32</sup>C.-M. Ma and A. E. Nahum, "Bragg-Gray theory and ion chamber dosimetry for photon beams," *Phys. Med. Biol.* **36**, 413–428 (1991).